JOURNAL OF PROPULSION AND POWER
Vol. 10, No. 6, Nov.–Dec. 1994

Numerical Study of the Performance of Swept, Curved Compression Surface Scramjet Inlets

John J. Korte*
NASA Langley Research Center, Hampton, Virginia 23681
D. J. Singh†
Analytical Services and Materials Inc., Hampton, Virginia 23666
Ajay Kumar‡
NASA Langley Research Center, Hampton, Virginia 23681
and
Aaron H. Auslender§
Lockheed Engineering and Sciences Company, Inc., Hampton, Virginia 23666

A computational performance enhancement study was performed employing systematic modifications to a planar-sidewall compression scramjet inlet operating at an entrance Mach number of 4 and at a dynamic pressure of 2040 psf. The variations included modifying the planar-sidewall compression angle as a function of height, utilizing sidewall curvature, and employing, simultaneously, both forward-swept and reverse-swept compression surfaces. Turbulent flowfield solutions were generated by solving the Reynolds-averaged Navier-Stokes equations to obtain inlet performance parameters such as total-pressure recovery, mass capture, and flowfield pressure distortion (the ratio of maximum static pressure to minimum static pressure generated at the inlet exit plane). Additionally, an inviscid parametric study was performed by employing solutions to the Euler equations to optimize a cubic polynomial that defined the longitudinal sidewall geometry. A final viscous flowfield solution of the optimized inviscid inlet geometry yielded inlet performance improvements; however, inlet top-wall surface boundary-layer shock wave separation interactions persisted. Hence, this numerical study demonstrated that enhanced performance is obtainable via curved-wall geometric modifications to the standard planar-sidewall inlet design, although future work should employ constraints to mitigate detrimental flow separation effects.

Nomenclature

A	=	cross-sectional area
CR	=	geometric contraction ratio
DI	=	distortion indicator
G	=	inlet throat width
H	=	inlet height
M	=	Mach number
p	=	pressure
T	=	temperature
u	=	streamwise velocity
W	=	initial inlet width
x, y, z	=	Cartesian coordinates
y^+	=	dimensionless law-of-the-wall parameter
ρ	=	density

Subscripts

a	=	average quantity
t	=	stagnation condition
1	=	freestream condition

Presented as Paper 93-1837 at the AIAA/SAE/ASME/ASEE 29th Joint Propulsion Conference and Exhibit, Monterey, CA, June 28–30, 1993; received Aug. 30, 1993; revision received March 16, 1994; accepted for publication March 21, 1994. Copyright © 1993 by the American Institute of Aeronautics and Astronautics, Inc. No copyright is asserted in the United States under Title 17, U.S. Code. The U.S. Government has a royalty-free license to exercise all rights under the copyright claimed herein for Governmental purposes. All other rights are reserved by the copyright owner.

*Senior Research Scientist, Theoretical Flow Physics Branch, Fluid Mechanics Division. Senior Member AIAA.
†Senior Research Scientist. Member AIAA.
‡Head, Theoretical Flow Physics Branch, Fluid Mechanics Division. Fellow AIAA.
§Principal Engineer.

Introduction

FOR over two decades, researchers have investigated, both experimentally and numerically, a number of highly integrated scramjet inlet concepts.[1–3] The majority of these inlet configurations were modular and designed with a fixed geometric, rectangular cross section. The flowfield compression is achieved by employing swept-planar sidewalls. The sweep of the sidewalls, in combination with the aft placement of the cowl on the underside of the inlet, allows for an efficient capture process to be maintained over a wide range of operating Mach numbers and for control of inlet starting characteristics. Although this approach has resulted in successful inlet configurations, there are numerous inlet design issues requiring further investigation such as top-wall separation problems, side-wall separation phenomena attributed to shock wave/boundary-layer interactions, corner flowfield control, reduction in flowfield nonuniformities, mitigation of blockage within the throat region due to viscous effects, excessive pressure rise near the cowl leading edge, and shock wave coalescence. Some improvements in the overall flowfield quality and performance have been obtained by using a combination of backward and forward sweep on the sidewalls[4,5]; however, the general improvement of this scramjet inlet design class has been hampered by the lack of an efficient and general three-dimensional design methodology.

Experimental investigations of alternate design concepts are expensive and time consuming due to the cost and effort associated with both building the test model and operating a hypersonic test facility. While numerical investigations are typically less expensive than experimental studies, the computational requirements are not trivial for solving the three-dimensional Navier-Stokes equations relevant to a flight-type integrated scramjet inlet. For example, expended CPU time for a numerical solution pertinent to the scramjet inlet ge-

ometry considered in this study is approximately 15 h on a Cray Y-MP. Therefore, not only a three-dimensional design methodology is needed, but also a more efficient method of evaluating design modifications.

In order to further address the problem areas previously discussed, the present study first analyzes three candidate design modifications to the baseline swept-planar sidewall compression inlet. This study focuses on a Mach number of 4 to enhance previously conducted computational and experimental efforts and is compatible with experimental facilities available to verify the improved inlet designs. Turbulent flowfield solutions are computed by solving the Reynolds-averaged Navier-Stokes equations in order to obtain the performance of the inlet. To assess the effect of viscous losses, solutions to the Euler equations are also generated for each inlet configuration. The three-dimensional Euler algorithms are very computationally efficient, with Cray Y-MP CPU time expenditures of less than 3 min typically being required to generate a solution. For the freestream conditions considered, the results of the inviscid performance predictions demonstrated the same trends as the Navier-Stokes predictions. In order to more systematically assess designing optimal sidewall compression inlets, Euler flowfield solutions are used to numerically explore the multidimensional parameter design space. To demonstrate the utility of this simplified technique, a two-parameter swept-curved sidewall inlet employing the inviscid flowfield equations is designed and optimized for both maximum total-pressure recovery and minimum flowfield pressure distortion. However, upon a comprehensive Navier-Stokes verification analysis to confirm enhanced inlet performance, top-wall surface flowfield separation is detected in the inviscidly derived optimal configuration. This separation indicates the requirement to implement a constrained Euler optimization procedure in order to adequately address this class of inlet geometries and flowfield physics.

Inlet Geometries

A salient feature of a swept-sidewall inlet geometry is that the shock/boundary-layer interactions do not occur in a plane perpendicular to the flow. This reduces the magnitude of the flowfield separation zones, if present, but increases the inlet sensitivity to oblique boundary-layer separation effects. Yet overall, this three-dimensional methodology has proven to be useful for designing inlets compatible with multiple flight-regime requirements. Specifically, integrated high-speed inlet designs must provide efficient high Mach number flowfield compression, as well as be functional in the low-speed flight regimes, i.e., exhibit reasonable starting characteristics and possess the ability to support a large back pressure during subsonic and dual-mode combustor operation. Inlet starting,

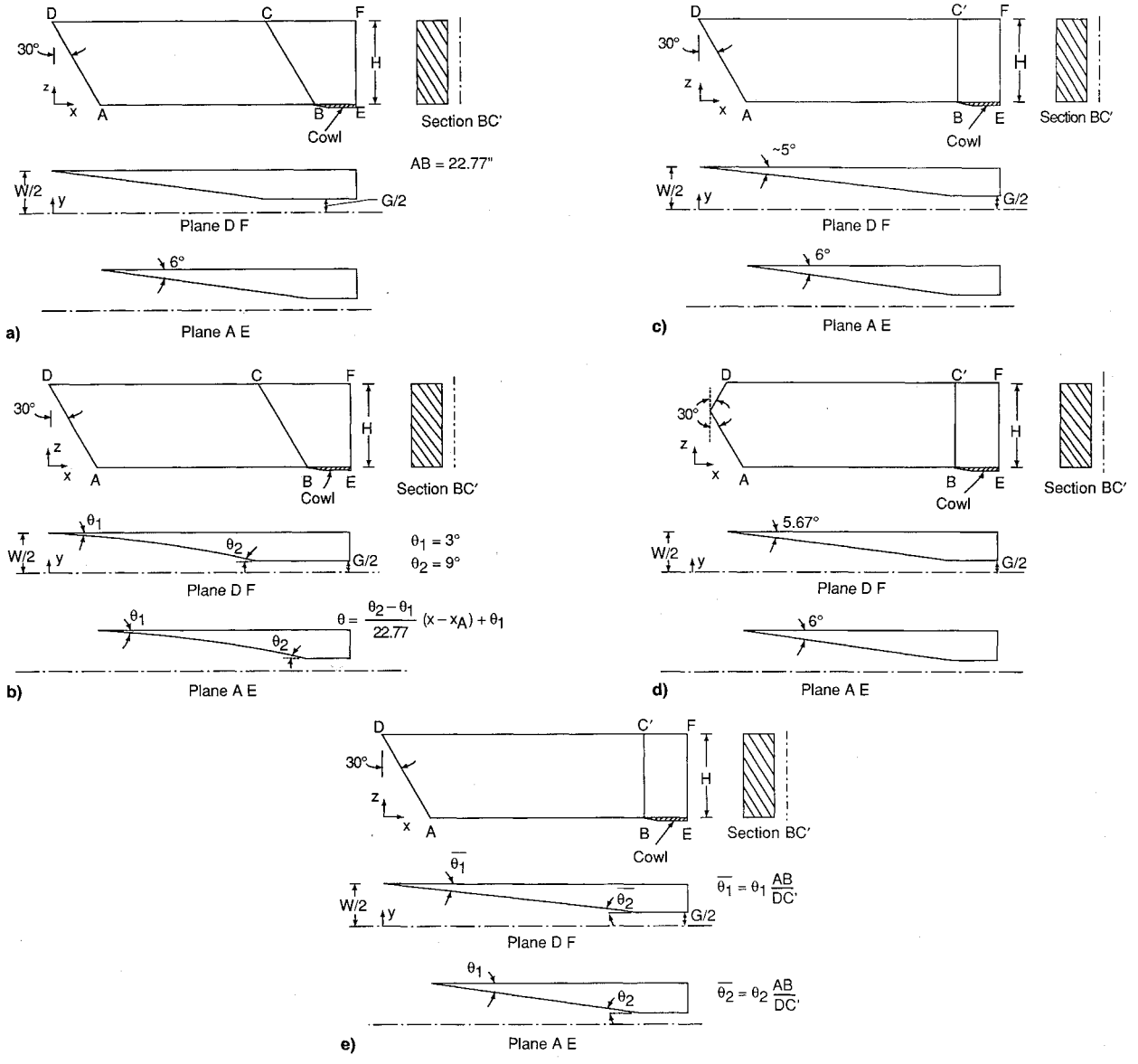

Fig. 1 Scramjet inlet configuration geometries: a) configuration A, b) configuration B, c) configuration C, d) configuration D, and e) configuration E.

mainly a low-speed flowfield spillage issue, is typically controlled for this class of modest contraction ratio fixed-geometry inlets by implementing swept-sidewall compression along with judicious aft cowl placement. Unfortunately, the solution to the low-speed starting problem typically hinders the high-speed performance characteristics of the inlet since the flowfield down turning required for inlet starting manifests as undesirable high-speed flowfield distortion. Also, this effect generally limits the back pressure capability of the inlet in the low-speed regimes via increased top-wall boundary-layer separation sensitivity. Thus, to partially assess these integrated inlet design considerations a numerical parametric study of three-dimensional inlet geometries was performed.

The various scramjet inlet geometries considered in this study are shown in Fig. 1. Figure 1a shows the baseline planar-compression surface inlet (configuration A). The sidewalls are swept at an angle of 30.0 deg and have a compression angle of 6.0 deg. Note that the sidewall sweep terminates along the line denoted as BC. This compression region is followed downstream by a constant area rectangular throat section. In this investigation the cowl, a potentially variable geometry inlet feature, is geometrically positioned at the location marked B. The inlet is designed with a geometric contraction ratio ($CR = W/G$) of 4.0, a width W of 6.4 in., and a height H of 7.2 in. Other dimensions are shown in the figure along with the inlet coordinate system.

Figure 1b shows configuration B, a curved surface inlet considered in this analysis. This inlet design is geometrically similar to configuration A, differing in that, in the streamwise direction, the sidewalls are parabolic in shape and are initiated with a 3.0-deg compression angle that increases linearly to 9.0 deg along the sweep line, denoted as BC. The second variation of the baseline inlet, configuration C, is presented in Fig. 1c. In this configuration the leading-edge sweep of the sidewalls gradually decreases to zero at the throat sweep line, denoted as BC′. Consequently, this results in a geometry for which each horizontal plane has a unique compression angle, varying from 6.0 deg in the cowl plane to nearly 5.0 deg in the top-wall plane. The fourth configuration, configuration D, is illustrated in Fig. 1d and is similar to configuration C, except that 30% of each inlet sidewall has reverse sweep. Each swept edge starts with an initial sweep angle of 30.0 deg and gradually reduces the sweep to 0 deg along the throat sweep line denoted as BC′. The final configuration examined in this study is shown in Fig. 1e and utilizes sidewall contours defined by a single cubic equation, but with the streamwise sidewall length scale functionally dependent upon height. Similar to configuration C, the top and bottom sidewall surfaces terminate along the same vertical plane.

Numerical Methods

Three-dimensional Navier-Stokes solutions for scramjet inlets A-E are obtained using the SCRAMIN code.[6] This computer code solves the Reynolds-averaged conservative form of the Navier-Stokes equations, formulated in a generalized coordinate system, employing the explicit algorithm of MacCormack.[7] Eddy viscosity is determined using the Baldwin-Lomax[8] turbulence model. The numerical analysis utilizes a finite-difference grid that is clustered near the inlet walls using algebraic stretching functions. The thermodynamic flowfield properties are modeled as calorically perfect, and Sutherland's law is used to compute the associated molecular viscosity. In prior investigations this code has been employed to numerically simulate swept-sidewall compression inlet processes, and the flowfield solutions favorably compared to experimental results.[9,10]

Three-dimensional Euler solutions for the integrated scramjet inlets are obtained using the explicit upwind space-marching algorithm previously developed for solving the parabolized Navier-Stokes equations.[11] For this study, this algorithm is simplified to solve only the Euler equation set by implementing slip-wall boundary conditions and eliminating the viscous-stress related quantities from the Navier-Stokes equations. The advantage of this approach is that the three-dimensional inviscid inlet flowfield solutions are obtained very quickly using a Cray Y-MP, thus allowing parametric studies to be accomplished efficiently.

The investigated configurations are numerically analyzed assuming either a fully turbulent or a completely inviscid inlet flowfield. The inlet surfaces are treated as adiabatic. The

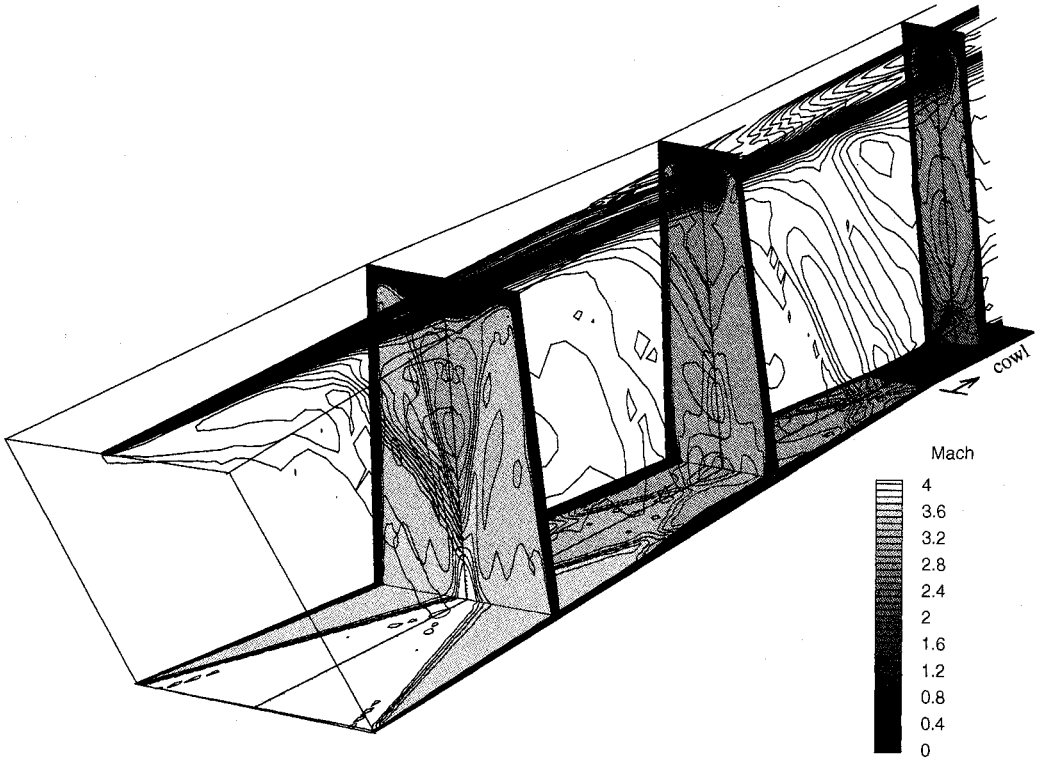

Fig. 2 Scramjet inlet flowfield Mach number contours (symmetry plane, cowl plane, and three cross-sectional planes).

viscous calculations employ a numerical grid of 51 points in the horizontal direction extending from the symmetry plane to the sidewall, 61 points in the vertical direction, and 93 points in the streamwise direction. For the turbulent analysis the grid is clustered at the boundaries to obtain a y^+ of less than 4 in the throat region. Seventeen of the grid points in the vertical direction are placed below the cowl plane to allow for an accurate simulation of the flowfield spillage occurring upstream of the cowl. The numerical grid for each inviscid calculation is identical in the crossflow plane, and subsequent to the generation of the space-marched inviscid analysis, the flowfield is mapped onto the reduced viscous grid. This procedure allows for a direct spatial flowfield comparison of identical inlet geometries using the two different solution techniques, and is required since the inviscid solution generates approximately 2000 planar crossflow data sets in the streamwise direction.

Results and Discussion

The performance of a planar-sidewall compression scramjet inlet is computationally investigated at the aerodynamic inflow conditions corresponding to an entrance Mach number of 4, a dynamic pressure of 2040 psf, and a static pressure and static temperature of 182 psf and 126°R, respectively. The inlet geometries for the various analyzed configurations have a geometric contraction ratio ($CR = W/G$) of 4.0, a width W of 6.4 in., a height H of 7.2 in., and consequently an aspect ratio of 4.5 (the ratio of the throat height to throat width). The inlet length scale is approximately 25 in. and is characterized by the value of 4 for the inlet length-to-height ratio.

First, in the subsequent text, the flowfield features typical of the baseline configuration are reviewed, followed by performance predictions for configurations A–D, based upon both viscous and inviscid analyses. The definitions of the various performance parameters utilized in this study are given in the Appendix. Second, a new inlet design is obtained by implementing a parametric optimization procedure based on Euler analysis, and the results are presented along with the associated viscous performance predictions.

Typical Inlet Flow Features

Typical swept-sidewall inlet flowfield features are seen in Fig. 2, where Mach number contours of the baseline configuration obtained from a Navier-Stokes analysis are illustrated. The symmetry plane, cowl plane, and three cross-sectional flowfield planes detail the overall shock wave and boundary-layer structure. The swept sidewall directs the flow towards the cowl plane, away from the inlet top wall. This aggravates the top-wall separation problem, mainly caused by the glancing shock interaction of the thickening top-wall boundary layer with the sidewall leading-edge shock wave. Additionally, the computational simulation predicts that the sidewall shock wave interaction structure aligns itself with the inlet sweep angle and traverses the vertical symmetry plane several times, decreasing total-pressure recovery and flowfield Mach number with each intersection. Hence, the resulting net inlet compression flowfield is a complex three-dimensional structure possessing numerous shock/shock and shock/boundary-layer interactions.

Performance Comparisons of Inlet Geometries A–D

The performance parameters derived from the viscous and inviscid flowfield analyses are listed in Table 1 and Table 2, respectively. Note that these values follow similar performance trends, and are obtained in a cross-sectional flowfield plane approximately 2 in. downstream of the inlet throat.

Examination of the resultant data presented in Table 1 indicates that configurations B, C, and D all perform better than the baseline configuration A in terms of mass capture, total-pressure recovery, and average static pressure ratio. The total-pressure recovery for configuration B is the highest, but this configuration has the worst value of the distortion parameter DI due to the large expansion that the flowfield undergoes along the throat sweep line, whereas configurations C and D have lower distortion values, concurrent with higher values of average static pressure ratio. In summary, configuration D yields superior performance results for multiple performance parameters and is characterized by a mass capture ratio of 82.3%, a total-pressure recovery ratio of 85.7%, an average static pressure ratio of 8.91, and a flowfield pressure distortion parameter of 2.08.

Table 1 Comparison of inlet performance at Mach 4 for turbulent flow, 2 in. downstream of the throat

Inlet configuration	A	B	C	D
Mass capture, %	76.9	80.8	80.5	82.3
M_a	2.47	2.45	2.41	2.38
P_{t_a}/p_{t_1}, %	84.9	88.1	86.3	85.7
p_a/p_1	7.77	8.25	8.66	8.91
Maximum pressure/p_1	17.1	17.8	13.3	13.4
Minimum pressure/p_1	5.33	4.57	6.06	6.44
DI	3.21	3.90	2.20	2.08

Table 2 Comparison of inlet performance at Mach 4 for inviscid flow, 2 in. downstream of the throat

Inlet configuration	A	B	C	D
Mass capture, %	81.0	84.8	84.2	85.2
M_a	2.70	2.68	2.67	2.68
p_{t_a}/p_{t_1}, %	93.8	97.3	95.4	95.3
p_a/p_1	6.42	6.79	6.74	6.63
Maximum pressure/p_1	13.8	13.7	10.6	10.0
Minimum pressure/p_1	4.39	3.39	4.01	3.83
DI	3.14	4.05	2.63	2.61

One aerodynamic performance issue investigated in this study, that of high-speed flowfield nonuniformity, is successfully addressed in configuration C by influencing the flowfield through the implementation of a variable sidewall compression angle as a function of inlet height. Another successful geometric variant, reverse-swept inlet configuration D, is also designed to modify the inlet pressure gradients and thereby decrease high-speed flowfield distortion. Both of the modified inlet designs, when analyzed with viscous effects, result in approximately a one-third reduction in the flowfield pressure distortion parameter. Additionally, these design modifications addressing flowfield nonuniformity are advantageous in resolving low-speed inlet back pressure limitations. This mutual benefit occurs since the redistribution of mass flux away from the cowl and towards the inlet top-wall surface aids in the reduction of top-wall boundary-layer separation.

Forebody Boundary-Layer Effects

To investigate the effects of boundary-layer ingestion, Navier-Stokes inlet flowfield solutions were computed for configurations A–D, employing inflow boundary conditions consistent with a turbulent forebody flowfield. The specified boundary-layer thickness is approximately 10% of the inlet height and emanates from a virtual sharp leading edge followed by a flat-plate forebody. The associated performance degradation varies from a 1–3% decrease in mass capture and from a 1–4% decrease in total-pressure recovery. These reductions are not deemed excessive; however, the influence of the ingested boundary layer is not well quantified and remains an issue for further investigation. The specific performance data relevant to this aspect of the study are given in Table 3.

Inviscid Design and Optimization

A logical approach to the design of three-dimensional inlets is to couple an optimization algorithm with a CFD flowfield solution algorithm that simulates all of the relevant flowfield physics. Optimization methodologies requiring multiple flowfield solutions are being investigated by numerous research-

Table 3 Comparison of inlet performance at Mach 4 for turbulent flow, 2 in. downstream of the throat (including forebody boundary layer)

Inlet configuration	A	B	C	D
Mass capture, %	74.8	79.7	79.8	81.5
M_a	2.44	2.46	2.37	2.32
p_{t_a}/p_{t_1}, %	82.2	87.0	83.5	82.3
p_a/p_1	7.45	7.79	8.47	9.02
Maximum pressure/p_1	19.3	18.9	14.7	16.7
Minimum pressure/p_1	4.45	3.84	6.22	5.41
DI	4.33	4.92	2.36	3.08

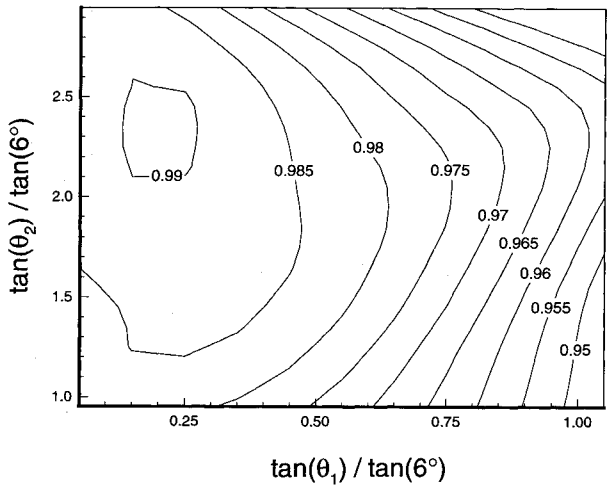

Fig. 3 Cubic sidewall inlet total-pressure recovery contours as a function of initial and final sidewall compression angles.

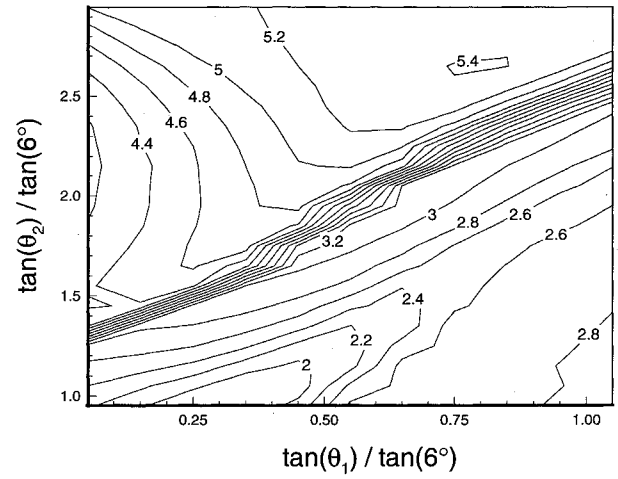

Fig. 4 Cubic sidewall inlet flowfield pressure distortion parameter contours as a function of initial and final sidewall compression angles.

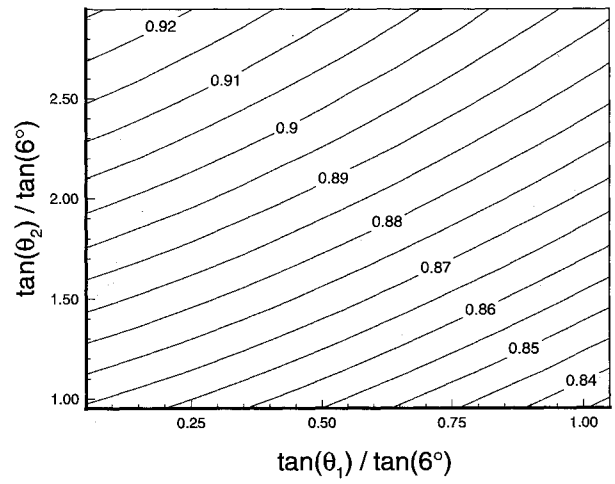

Fig. 5 Cubic sidewall inlet mass capture ratio contours as a function of initial and final sidewall compression angles.

ers. Generally, these techniques would demand enormous computational capability to numerically address the inlet flowfields considered in this study, since multiple solutions of the three-dimensional Navier-Stokes equations would be required. Additional analytic difficulties include the establishment of the appropriate inlet performance figures-of-merit and the problem of efficiently defining a parametric representation of the inlet surface geometry. A partial step towards developing a comprehensive three-dimensional CFD-based design/optimization procedure for scramjet inlets is to employ approximations to the Navier-Stokes equations. Thus, an efficient inviscid algorithm has been used in this study to generate flowfield solutions for the three-dimensional inlet optimization process. As presented in the parametric viscous results, the inviscid approach yields similar inlet performance trends.

In this study, the figures-of-merit employed in the optimization procedure are the maximization of the inlet total-pressure recovery and the minimization of the flowfield pressure distortion parameter. The inlet optimization procedure works with two geometric parameters, the initial sidewall compression angle and final sidewall compression angle, and hence, uniquely determines the cubic polynomial that defines the sidewall aerodynamic geometry (Fig. 1e).

To obtain the optimum inviscid design, a matrix of 231 solutions is generated to explore inlet performance as a function of these two inlet design parameters. The relevant results, momentum-averaged total-pressure recovery, flowfield pressure distortion parameter, and mass capture at the exit of the inlet, are shown, using contour plots, in Figs. 3, 4, and 5, respectively. Note that the total-pressure ratio recovery function (Fig. 3) has a plateau value of nearly 99% at an initial sidewall compression angle of approximately 1.2 deg and a final sidewall compression angle of 13.6 deg, as measured in the cowl plane. Concurrently, the pressure distortion parameter (Fig. 4) reaches a minimum of 1.81 at an initial sidewall compression angle of approximately 1.5 deg and a final sidewall compression angle of 5.7 deg, as measured in the cowl plane. The mass capture is nearly a linear function that increases with a decreasing initial sidewall compression angle and an increasing final sidewall compression angle (Fig. 5). The optimal values for the two inlet design parameters are 1.50 deg for the initial sidewall compression angle and 6.32 deg for the final sidewall compression angle. These values result from the selection of an inlet geometry yielding, as measured from optimal performance criteria, nearly a 10% increase in the distortion parameter and a less than 1% reduction in the total-pressure recovery. Note that this result is based only on inviscid performance predictions and is not constrained by viscous flow criteria.

Viscous Assessment of Optimized Design

A Navier-Stokes flowfield solution is computed using the inviscidly derived optimized geometry (configuration E). Results indicate an improvement in total-pressure recovery compared with the baseline, configuration A, and all other examined configurations (B–D). The top-wall boundary-layer separation issue associated with the inviscidly derived optimal configuration is evident upon examination of Mach number contours in the midhorizontal plane of the inlet (Fig. 6a), in the cross-sectional flowfield plane approximately 2 in. down-

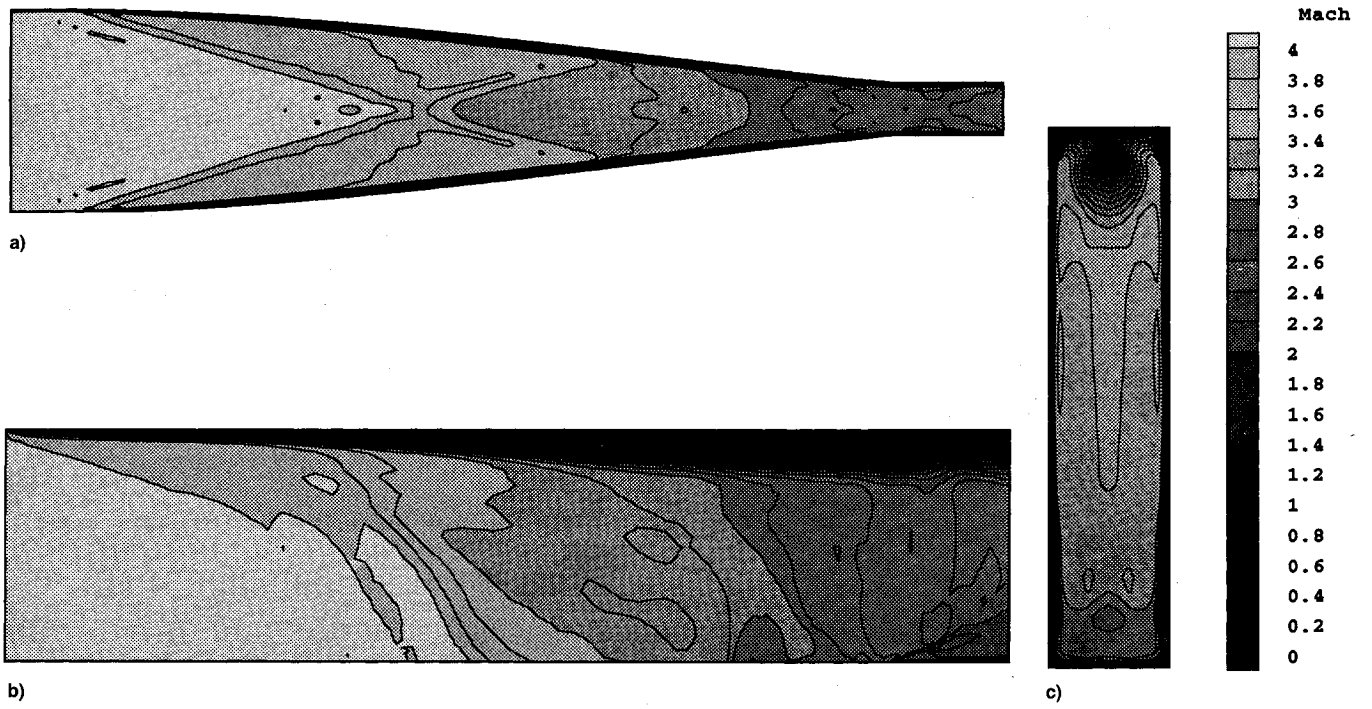

Fig. 6 Computed Navier-Stokes Mach number contours for the inviscidly optimized inlet design: a) midhorizontal plane, b) symmetry plane, and c) cross-sectional flowfield plane approximately 2 in. downstream of the throat.

stream of the throat (Fig. 6b), and in the symmetry plane of the inlet (Fig. 6c). A top-wall separation region is present in configuration E, demonstrating one difficulty of employing the reduced Euler equation set to obtain an overall optimal design. An alternative approach for utilizing the Euler equations in a design methodology is to incorporate a constraint function implemented concurrently with the optimization process, which would limit the local flowfield phenomena in such a manner so as to minimize or eliminate separation effects. Since this latter approach is not utilized in this investigation, the total potential for performance enhancement has not yet been realized. However, configuration E does yield a flowfield structure resulting in inlet performance improvements characterized by a mass capture ratio of 84.3%, a total-pressure recovery ratio of 90.1%, and a flowfield pressure distortion parameter of 2.78.

Summary

A numerical study was conducted to assess the performance impacts of sidewall contour modifications to a baseline swept-sidewall compression scramjet inlet operating at an entrance Mach number of 4. The effect of implementing sidewall curvature, altering the planar-sidewall compression angle as a function of height, and employing, simultaneously, both forward-swept and reverse-swept compression surfaces, demonstrated selective performance enhancements via flowfield mass-flux redistribution towards the inlet top-wall surface. Additionally, the inviscid and viscous analyses of identical inlet geometry sets demonstrated similar inlet performance trends.

In an attempt to develop a more systematic three-dimensional scramjet inlet design procedure, a sidewall compression inlet geometry was obtained by optimizing performance for a two-parameter inlet design utilizing flowfield analysis based upon the Euler equations. Although the viscous flowfield solution for the inviscidly optimized curved-sidewall configuration yielded inlet top-wall boundary-layer separation (as did the baseline), it still exhibited an improvement in performance compared to the baseline planar-sidewall inlet design. Thus, this computational investigation demonstrates the utility of employing nonplanar three-dimensional inlet design methodologies, and that a viscously constrained optimization procedure should be employed in conjunction with an efficient fluid dynamic solution algorithm to achieve overall optimal scramjet inlet performance.

Appendix: Performance Parameters

The performance quantities used in Tables 1–3 for a cross section in the throat region are defined as follows:

Momentum-averaged Mach number

$$M_a = \frac{\int_A \rho u^2 M \, dA}{\int_A \rho u^2 \, dA} \tag{A1}$$

Momentum-averaged total-pressure recovery

$$\frac{p_{t_a}}{p_{t_1}} = \frac{\int_A \rho u^2 p_t / p_{t_1} \, dA}{\int_A \rho u^2 \, dA} \tag{A2}$$

Area-weighted compression ratio

$$p_a/p_1 = \frac{\int_A p/p_1 \, dA}{\int_A dA} \tag{A3}$$

Distortion indicator

$$DI = \frac{\max(p/p_1)}{\min(p/p_1)} \tag{A4}$$

References

[1]Trexler, C. A., "Inlet Starting Predictions for Sidewall Compression Scramjet Inlets," AIAA Paper 88-3257, July 1988.

[2]Trexler, C. A., "The Design and Performance at Mach 4.0 of

Two-Strut Hypersonic Inlets for an Integrated Scramjet Concept," NASA TM-4022, May 1988.

[3]Kumar, A., "Numerical Simulation of Flow Through a Two-Strut Scramjet Inlet," *Journal of Propulsion and Power*, Vol. 5, No. 3, 1989, pp. 341–345.

[4]Weidner, J. P., Trexler, C. A., Carr, J., and Kumar, A., "Opposite Sweep Sidewall Compression Inlet Research at NASA Langley Research Center (U)," 8th National Aero-Space Plane Symposium, Paper 15a, Monterey, CA, March 1990.

[5]Kumar, A., Singh, D. J., and Trexler, C. A., "Numerical Study of the Effects of Reverse Sweep on Scramjet Inlet Performance," *Journal of Propulsion and Power*, Vol. 8, No. 3, 1992, pp. 714–719.

[6]Kumar, A., "Numerical Simulation of Scramjet Inlet Flow Fields," NASA TP-2517, May 1986.

[7]MacCormack, R. W., "The Effect of Viscosity in Hypervelocity Impact Cratering," AIAA Paper 69-354, April 1969.

[8]Baldwin, B., and Lomax, H., "Thin Layer Approximation and Algebraic Model for Separated Turbulent Flows," AIAA Paper 78-0257, Jan. 1978.

[9]Holland, S. D., "A Computational and Experimental Investigation of a Three-Dimensional Hypersonic Scramjet Inlet Flow Field," Ph.D. Dissertation, North Carolina State Univ., Raleigh, NC, 1991.

[10]Singh, D. J., Trexler, C. A., and Hudgens, J. A., "Three-Dimensional Simulation of a Translating Strut Inlet," *Journal of Propulsion and Power*, Vol. 10, No. 2, 1994, pp. 191–197.

[11]Korte, J. J., "An Explicit Upwind Algorithm for Solving the Parabolized Navier-Stokes Equations," NASA TP 3050, Feb. 1991.

REVISED AND ENLARGED!

AIAA Aerospace Design Engineers Guide

Third Edition

This third, revised and enlarged edition provides a condensed collection of commonly used engineering reference data specifically related to aerospace design. It's an essential tool for every design engineer!

TABLE OF CONTENTS:

Mathematics • Section properties • Conversion factors • Structural elements • Mechanical design
Electrical/electronic • Aircraft design • Earth, sea and solar system • Materials and specifications
Spacecraft design • Geometric dimensioning and tolerancing

1993, 294 pp, illus, 9 x 3⅛" leather-tone wire binding, ISBN 1-56347-045-4
AIAA Members $ 29.95, Nonmembers $49.95, Order #: 45-4(945)

Place your order today! Call 1-800/682-AIAA

AIAA
American Institute of Aeronautics and Astronautics

Publications Customer Service, 9 Jay Gould Ct., P.O. Box 753, Waldorf, MD 20604
FAX 301/843-0159 Phone 1-800/682-2422 9 a.m. - 5 p.m. Eastern

Sales Tax: CA residents, 8.25%; DC, 6%. For shipping and handling add $4.75 for 1-4 books (call for rates for higher quantities). Orders under $100.00 must be prepaid. Foreign orders must be prepaid and include a $20.00 postal surcharge. Please allow 4 weeks for delivery. Prices are subject to change without notice. Returns will be accepted within 30 days. Non-U.S. residents are responsible for payment of any taxes required by their government.